for which charge-density studies have been reported by Marumo, Isobe, Saito, Yagi & Akimoto (1974) and by Marumo, Isobe & Akimoto (1977). The geometries of the structures become progressively farther from ideal through the series M = Ni, Co, Fe. The satellites are very weak in the Ni complex. In the Fe complex, which has a more distorted geometry, the d-electron maxima show a pronounced difference in height, and there are strong satellites associated with the larger maxima.

The development of the satellite peaks may be related to the requirements of the state function for ideal and non-ideal geometries. An atomic $3d$ function has a single maximum in the radial direction. Except for the node at the origin there are no radial nodes in the $3d$ density function. This is characteristic of the densities observed for transition-metal complexes with nearly ideal geometries.

For structures with non-ideal geometries s- and p-type contributions to the valence density may occur. These terms have more radial structure than $3d$ functions, accounting for the subsidiary maxima in $\Delta\rho$ maps for these less-symmetrical structures.

A Perkin-Elmer 3240 computer was used for all calculations. Standard programs from the *XTAL* system (Stewart & Hall, 1985) were used in the structure refinement and for evaluating the difference density. Financial support for this project was provided by the Australian Research Grants Scheme and by the Research Committee of the University of Western Australia. One of us (SCR) acknowledges receipt of a Commonwealth Postgraduate Award.

References

CHANTLER, C. (1985). *PARTN.* Listing and documentation. Unpublished.
HIRSHFELD, F. (1977). *Theor. Chim. Acta*, **44**, 129-138.
International Tables for X-ray Crystallography (1974). Vol. IV. Birmingham: Kynoch Press. (Present distributor D. Reidel, Dordrecht.)
IWATA, M. & SAITO, Y. (1973). *Acta Cryst.* B**29**, 822-832.
KIJIMA, N., TANAKA, K. & MARUMO, F. (1981). *Acta Cryst.* B**37**, 545-548.
KIJIMA, N., TANAKA, K. & MARUMO, F. (1983). *Acta Cryst.* B**39**, 557-561.
MARUMO, F., ISOBE, M. & AKIMOTO, S. (1977). *Acta Cryst.* B**33**, 713-716.
MARUMO, F., ISOBE, M., SAITO, Y., YAGI, T. & AKIMOTO, S. (1974). *Acta Cryst.* B**30**, 1904-1906.
MASLEN, E. N., RASTON, C. L., SKELTON, B. W. & WHITE, A. H. (1975). *Aust. J. Chem.* **28**, 739-744.
MASLEN, E. N., RIDOUT, S. C. & WATSON, K. J. (1987). In preparation.
MASLEN, E. N., SPADACCINI, N. & WATSON, K. J. (1983). *Proc. Indian Acad. Sci.* **92**, 443-448.
MASLEN, E. N., SPADACCINI, N., WATSON, K. J. & WHITE, A. H. (1986). *Acta Cryst.* B**42**, 430-436.
MIYATA, N., TANAKA, K. & MARUMO, F. (1983). *Acta Cryst.* B**39**, 561-564.
OHBA, S. & SAITO, Y. (1984). *Acta Cryst.* C**40**, 1639-1641.
OHBA, S., SATO, S., SAITO, Y., OHSHIMA, K.-I. & HARADA, J. (1983). *Acta Cryst.* B**39**, 49-53.
REES, B. (1977). *Isr. J. Chem.* **16**, 180-186.
SPACKMAN, M. A. & MASLEN, E. N. (1986). *J. Phys. Chem.* **90**, 2020-2027.
STERNHEIMER, R. (1950). *Phys. Rev.* **78**, 235-243.
STEVENS, E. D. & COPPENS, P. (1979). *Acta Cryst.* A**35**, 536-539.
STEWART, J. M. & HALL, S. R. (1985). *The XTAL System of Crystallographic Programs.* Tech. Rep. TR-1364.1. Computer Science Center, Univ. of Maryland, College Park, Maryland.
TREFRY, M. G., MASLEN, E. N. & SPACKMAN, M. A. (1987). *J. Phys. C*, **20**, 19-28.
VARGHESE, J. N. & MASLEN, E. N. (1985). *Acta Cryst.* B**41**, 184-190.

Acta Cryst. (1987). B**43**, 356-368

Structural Analysis of the Incommensurate and Lock-in Phases of Tetramethylammonium Tetrachlorozincate(II), $[N(CH_3)_4]_2[ZnCl_4]$

BY G. MADARIAGA, F. J. ZUÑIGA, J. M. PÉREZ-MATO AND M. J. TELLO

Departamento de Física, Facultad de Ciencias, Universidad del Pais Vasco, Apdo 644, *Bilbao, Spain*

(*Received* 29 *September* 1986; *accepted* 12 *February* 1987)

Abstract

The structures of the incommensurate and lock-in phases of $[N(CH_3)_4]_2[ZnCl_4]$ have been determined and analysed in terms of symmetry modes. X-ray diffraction intensities of the incommensurate phase, including first- and second-order satellites, were collected at 286·4 K. Refinements were performed in the superspace group $P(Pmcn)$:$(s, 1, -1)$ including in the modulation function harmonics up to second order. From a total of 475 independent reflections, final R values of 0·077, 0·052, 0·121 and 0·49 for all, main, first- and second-order reflections, respectively, were obtained. First-order harmonics dominate in the modulation, the most important component of the distortion being that parallel to the a axis. The refinements of the lock-in ferroelectric structure were performed in the space group $P2_1cn$, using as starting parameters those of the basic structure extended to five cells. A final $R = 0{\cdot}075$ for 917 observed reflec-

0108-7681/87/040356-13$01.50

tions was obtained. The transition from the incommensurate to the lock-in phase can be analysed in terms of symmetry modes which transform according to irreducible representations of the *Pmcn* space group. The symmetry mode decomposition of the distortion of the lock-in structure shows that the $\sum_3$ primary mode is predominant but B_{2u} and $\sum_2$ modes also have important amplitudes. The comparison between the incommensurate and lock-in distortions reveals a large correlation between them, the $\sum_3$ distortion mode being essentially the same in both structures. Crystal data: $M_r = 355{\cdot}5$, Cu $K\alpha$, $\lambda = 1{\cdot}54184$ Å, $\mu = 76{\cdot}3$ cm^{-1}. Incommensurate phase: $a = 8{\cdot}987$ (2), $b = 15{\cdot}503$ (2), $c = 12{\cdot}258$ (2) Å, $V = 1707{\cdot}9$ (9) Å^3, $Z = 4$, $D_x = 1{\cdot}38$ g cm^{-3}, $F(000) = 736$. Lock-in phase: $a = 8{\cdot}986$ (1), $b = 15{\cdot}484$ (3), $c = 61{\cdot}26$ (1) Å, $V = 8524$ (4) Å^3, $Z = 20$, $D_x = 1{\cdot}38$ g cm^{-3}, $F(000) = 3680$.

1. Introduction

Tetramethylammonium tetrachlorozincate(II) (TMATC-Zn), in common with other members of the A_2BX_4 family (see review of Iizumi, 1981), exhibits several phase transitions, the most important characteristic being the existence of a one-dimensional incommensurate (INC) phase followed by a ferroelectric phase. Starting from room temperature, TMATC-Zn presents five phase transitions:

$$\mathrm{I} \overset{297\ \mathrm{K}}{\underset{T_i}{\longrightarrow}} \mathrm{II} \overset{281\ \mathrm{K}}{\underset{T_c}{\longrightarrow}} \mathrm{III} \xrightarrow{277\ \mathrm{K}} \mathrm{IV} \xrightarrow{171\ \mathrm{K}} \mathrm{V} \xrightarrow{159\ \mathrm{K}} \mathrm{VI},$$

where the transition temperatures correspond to those obtained by calorimetric measurements by Ruiz-Larrea, Lopez-Echarri & Tello (1981). These transitions have been confirmed and studied by Brillouin (Karajamaki, Lacho & Levola, 1983), EPR (Machida, Suhara, Aono & Kobayashi, 1983), Raman (Henocque, Sauvajol, Lefebvre & Marion, 1983) and diffraction techniques (Marion, 1981; Almairac, Ribet, Ribet & Bziouet, 1980; Mashiyama & Tanisaki, 1980).

The crystal structure of phase I (basic structure) was solved by Wiesner, Srivastava, Kennard, Di Vaira & Lingafelter (1967). It is orthorhombic, space group *Pmcn* (standard *Pnma*), with $Z = 4$. The structure consists of tetrahedral $ZnCl_4$ ions located on the mirror planes m, bonded to $N(CH_3)_4$ groups located on the same planes. The projection of the structure in the *ac* plane is shown in Fig. 1. Remarkable in the refinement of Wiesner *et al.* are the high values of the atomic thermal parameters, showing the existence of an orientational disorder (Blinc, Burgar, Slak, Rutar & Milia, 1979), confirmed by the diffuse scattering observed in X-ray diffraction experiments. The amount of disorder seems to be less in the low-temperature phases.

The structure of phase II is an INC modulation of the basic structure, with a wave vector $\mathbf{k} = (\frac{2}{5} + \delta)\mathbf{c}^*$. Most of the reported X-ray (Almairac *et al.*, 1980; Marion, 1981; Mashiyama & Tanisaki, 1980) and neutron (Gesi & Iizumi, 1980) diffraction studies on the INC phase of this compound are devoted to the investigation of the temperature dependence of the modulation wavevector $\mathbf{k}$ and the satellite intensities. In the temperature stability range of this phase, δ has a smooth variation between 0·02 at the T_i transition temperature and 0·008 near T_c, jumping to 0 at T_c. The behaviour of the first-order satellite intensities follows a critical law $(T - T_i)^{2\beta}$ with $2\beta = 0{\cdot}74$.

In the next low-temperature phases, Tanisaki & Mashiyama (1980) have found that the cell parameter along the c axis changes from the value c_0 in the basic structure to $5c_0$, $3c_0$, c_0 and $3c_0$ in phases III, IV, V and VI, respectively. The corresponding symmetry changes are the following: the ferroelectric phase III is orthorhombic, space group $P2_1cn$ and $Z = 20$; phase IV is monoclinic, space group $P2_1/n$ (first setting) and $Z = 12$; phase V is monoclinic, space group $P2_1/c$ (second setting) and $Z = 4$; and finally phase VI is orthorhombic, space group $P2_12_12_1$ and $Z = 12$.

The structural changes associated with these transitions can be described by small distortions of the basic structure and the symmetry of the modes participating in these distortions can be calculated using group and Landau theories. To explain the sequence of transitions in TMATC-Zn, several phenomenological approaches based on a free-energy expansion, have been published (Mashiyama, 1980; Parlinski & Denoyer, 1985, and references therein). In this context, the microscopic characteristics of these phases are summarized as follows. The INC phase has an order parameter of $\sum_3$ symmetry in $\mathbf{k} = (\frac{2}{5} + \delta)\mathbf{c}^*$ (the notation employed for the irreducible representations is given in Table 1). Phase III is characterized by the

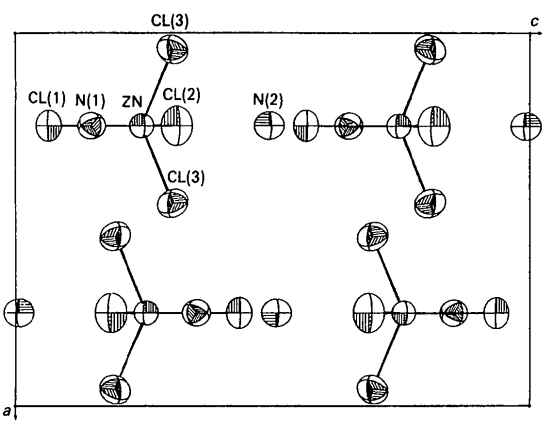

Fig. 1. *ac* projection of the basic structure of TMATC-Zn. For simplicity, only the N atoms of the tetramethylammonium groups are represented.

Table 1. *Character table of the little group at* $\sum$: $(0, 0, k)$

	$\{E\|0\,0\,0\}$	$\{C_{2z}\|\frac{1}{2}\frac{1}{2}\frac{1}{2}\}$	$\{\sigma_y\|0\frac{1}{2}\frac{1}{2}\}$	$\{\sigma_x\|\frac{1}{2}0\,0\}$
$\sum_1$	1	1	1	1
$\sum_2$	1	1	−1	−1
$\sum_3$	1	−1	1	−1
$\sum_4$	1	−1	−1	1

lock-in of the wave vector of the structural distortion at the value $\mathbf{k}=\frac{2}{5}\mathbf{c}^*$ (hereafter this phase is referred to as the lock-in phase). The distortion in this phase has been described with $\sum_3(\mathbf{k}=\frac{2}{5}\mathbf{c}^*)$ primary mode and two $\sum_2(\mathbf{k}=\frac{1}{5}\mathbf{c}^*)$ and B_{2u} $(\mathbf{k}=0)$ compatible modes, the second corresponding to the spontaneous polarization. The distortions of the threefold superstructures in phases IV and VI are described by $\sum_3(\mathbf{k}=\frac{1}{3}\mathbf{c}^*)$, B_{3g} $(\mathbf{k}=0)$ and $\sum_3(\mathbf{k}=\frac{1}{3}\mathbf{c}^*)$, A_u $(\mathbf{k}=0)$ modes respectively. Finally, phase V includes $\sum_3$ and B_{1g} (both in $\mathbf{k}=0$) modes in its distortion. This description is not sufficient to describe the microscopic characteristics, at least for the INC and lock-in phases, and in § 7 we shall discuss the relevance in these phases of some other modes of different symmetry.

In this work we report the structure determination of the INC and lock-in phases of TMATC-Zn. For the lock-in phase standard methods have been used, while in the INC phase superspace formalism has been considered. Since the introduction of this multidimensional description and the superspace-group concept by de Wolff (1974, 1977) and Janner & Janssen (1977, 1980), the analysis and description of INC structures have been drastically simplified. In particular, the *REMOS*.82 (Yamamoto, 1982*a*) program, written on the basis of the superspace symmetry and a multi-dimensional structure factor, has been successfully used by several authors to refine INC structures (Yamamoto, 1980; van Smaalen, Bronsema & Mahy, 1986). This was also the program employed in the present case. A subsequent comparison of the two determined structures allows one to check their mutual consistency and the relevance of the different symmetry modes in both structural distortions.

2. Experimental

Single crystals of TMATC-Zn were grown by slow evaporation at room temperature from an aqueous solution containing $N(CH_3)_4Cl$ and $ZnCl_2$ in stoichiometric proportions. Two 0·3 mm diameter spherical crystals were used to collect the data needed for structure refinement of the INC and lock-in phases. The X-ray diffraction intensities were measured with an automatic four-circle diffractometer (Syntex $P2_1$) using Ni-filtered Cu radiation. The diffractometer was equipped with an N_2-gas-flow low-temperature system and temperature was controlled by a thermocouple positioned at a distance of 2 mm from the crystal; stability in temperature was better than ±0·2 K. Intensities were measured by the θ–2θ scan technique with an intensity-dependent scan speed varying between 2 and 10 °min^{-1}. The background was evaluated by analysing the scan profile (Schwarzenbach, 1977). The standard deviation $\sigma(I)$ of the intensities was obtained from counting statistics.

2.1. *Phase INC*

A preliminary study of the INC phase at 288 K was made taking Weissenberg photographs of *h*0*l*, *h*1*l* and *h*2*l* layers. The modulation wave vector measured on these diagrams corresponds to a value of 0.41**c***, in accordance with previous reported values (Tanisaki & Mashiyama, 1980). The systematic extinctions for the main reflections are compatible with the *Pmcn* space group for the average structure but, owing to the small number of detected satellite reflections (which were only of the first-order type), systematic extinctions in these reflections for the superspace-group determination could not be established. As is explained below, the superspace group of the INC structure was determined from theoretical arguments.

The identification of the INC phase on the automatic diffractometer was made by centring and scanning the 200 reflection at different temperatures. Starting from room temperature and lowering it by steps of 0·5 K, we considered the INC phase to be reached when the reflection $2,0,\frac{2}{5}+\delta$, or 2001 in the four-index scheme (de Wolff, 1974), could be distinguished. As the temperature is decreased from T_i to T_c, two well-known features are observed: the increase of the satellite reflection intensities and the continuous variation of the modulation wave vector. Fig. 2 shows the behaviour with the temperature of the integrated intensities of $14\bar{2}\bar{1}$ and $15\bar{1}\bar{1}$ satellite reflections. The fit of these curves to a functional dependence $I\propto(T-T_i)^{2\beta}$ gives 2β values of 0·70 and 0·73 respectively, which are below the 0·74 value reported by Mashiyama & Tanisaki (1980).

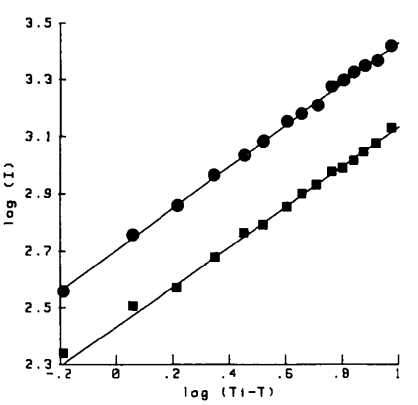

Fig. 2. Log–log plot of the intensity *versus* (T_i-T) of satellite reflections $14\bar{2}\bar{1}$ (●) and $15\bar{1}\bar{1}$ (■).

Integrated intensities were collected in the INC phase at an estimated temperature of 286·4 K, corresponding to a wave-vector value of $0{\cdot}413\mathbf{c}^*$. At this temperature, the lattice parameters of the average structure as determined by least-squares refinement of Bragg angles of 25 main reflections are $a=8{\cdot}987\,(2)$, $b=15{\cdot}503\,(2)$ and $c=12{\cdot}258\,(2)$ Å. Max. $2\theta=45°$. In order to include satellite reflections in the data collection, the diffractometer control program was modified introducing an additional satellite index. Three standard reflections, no intensity variation. 1283 reflections (including main reflections, first- and second-order satellites) were collected. $h=0$–3, $k=0$–7, $l=\bar{6}$–6, $m=\bar{2}$–2. Symmetric equivalent reflections were averaged and after elimination of satellite reflections with strong asymmetric background, $R_{\rm int}=0{\cdot}050$, a set of 475 independent reflections [304 observed with $I>3\sigma(I)$] was obtained and used in the refinements. To derive the moduli of structure factors, data were corrected for geometrical factors and an isotropic absorption correction was applied: min., max. absorption corrections = 4·708, 5·013.

2.2. *Lock-in phase*

The lock-in phase is stable in a narrow range of temperature (~3 K) and was detected by heating the crystal from phase IV until the $20\frac{1}{3}$ reflection (with index referred to the basic structure) vanished completely. Three standard reflections, no intensity variation. Max. $2\theta=45°$. Intensities were measured at about 278 K. At this temperature, the lattice constants of the superstructure were measured to be $a=8{\cdot}986\,(1)$, $b=15{\cdot}484\,(3)$ and $c=61{\cdot}26\,(1)$ Å. Intensity data for 4250 reflections were collected ($h=0$–4, $k=\bar{6}$–6, $l=\overline{40}$–40) and after averaging equivalent reflections, $R_{\rm int}=0{\cdot}048$, geometrical and absorption corrections were applied to 1238 independent reflections [917 observed $I>3\sigma(I)$]. Min., max. absorption corrections = 4·708, 5·013.

3. Superspace-group determination

As was mentioned before, owing to the weakness of the satellite reflection intensities, the superspace group of the INC phase could not be determined by observing systematic extinctions. However, the knowledge of the basic and lock-in space groups restricts the number of superspace groups to be considered.

With Landau theory, all possible space groups of the lock-in phase and the symmetry of the corresponding order parameters can be calculated; they are given in Table 2. As the space group of the lock-in phase is known to be $P2_1cn$, the symmetry and phase of the order parameter are unambiguously identified as $\sum_3$ and $\pi/2$ respectively. Owing to the continuity of the order parameter between the INC and lock-in phases, $\sum_3$ is also the irreducible representation according to which the order parameter of the INC phase transforms, having in this case an arbitrary phase. Once the symmetry of the order parameter of the INC phase is known, the generalized transformations that leave the order parameter invariant and form the superspace group of the INC structure can be determined using the formulation developed by Pérez-Mato, Madariaga & Tello (1984*a*,*b*). Accordingly, the fundamental elements of the required superspace group are:

Table 2. *Possible space groups for the lock-in phase at* $\frac{2}{5}\mathbf{c}^*$ *predicted by Landau theory*

	$\varphi=0$	$\varphi=\pi/2$	$\varphi\neq 0,\neq\pi/2$
$\sum_1$	$Pmcn$	$Pmcn2_1$	$Pmc2_1$
$\sum_2$	$P112_1/n$	$P2_12_12_1$	$P112_1$
$\sum_3$	$P12_1/c1$	$P2_1cn^*$	$P1c1$
$\sum_4$	$P2_1/m11$	$Pm2_1n$	$Pm11$

$$\begin{array}{lll}
\{E\,|\,0\,0\,0,\,n\}\,n\in Z & \{I\,|\,0\,0\,0,\,0\} & \{E\,|\,1\,0\,0,\,0\} \\
\{C_{2x}\,|\,\frac{1}{2}\,0\,0,\,\frac{1}{2}\} & \{\sigma_x\,|\,\frac{1}{2}\,0\,0,\,\frac{1}{2}\} & \{E\,|\,0\,1\,0,\,0\} \\
\{C_{2y}\,|\,0\,\frac{1}{2}\,\frac{1}{2},\,-\alpha/2\} & \{\sigma_y\,|\,0\,\frac{1}{2}\,\frac{1}{2},\,-\alpha/2\} & \{E\,|\,0\,0\,1,\,-\alpha\} \\
\{C_{2z}\,|\,\frac{1}{2}\,\frac{1}{2}\,\frac{1}{2},\,-\alpha/2+\frac{1}{2}\} & \{\sigma_z\,|\,\frac{1}{2}\,\frac{1}{2}\,\frac{1}{2},\,-\alpha/2+\frac{1}{2}\}, &
\end{array} \quad (1)$$

where the notation is as follows. If $\{R\,|\,t_x\,t_y\,t_z,\,\tau\}$ represent a general transformation, R and t_x, t_y, t_z are the rotational and translational parts performed in the three-dimensional real space and τ is the phase translation corresponding to the internal coordinate; $\alpha=|\mathbf{k}|/|\mathbf{c}^*|$, $\mathbf{k}$ being the modulation wave vector. In (1), the phase of the order parameter of the INC phase has been chosen arbitrarily as zero. Transformations (1) correspond, except for a phase translation of the modulation, to the superspace group $P(Pmcn):(s,1,-1)$ [No. 62*c*.9.2, in the notation of de Wolff, Janssen & Janner (1981)], in accordance with the superspace group recently considered by Dam & Janner (1986).

The superspace group $P(Pmcn):(s,1,-1)$ implies the following systematic extinction rules:

$$\begin{aligned}
h+k=\text{odd} \quad &\text{for } (h,k,0,0),\\
l=\text{odd} \quad &\text{for } (h,0,l,m),\\
m=\text{odd} \quad &\text{for } (0,k,l,m).
\end{aligned}$$

As stated above, the rules corresponding to satellite reflections could not be independently determined from the experimental data, but they are satisfied by all the observed reflections.

4. Description of an INC structure

We review here shortly, following Pérez-Mato, Madariaga, Zuñiga & Garcia Arribas (1987), the basic concepts for describing an INC structure and the

meaning of the structural parameters to be determined.

A displacive INC structure corresponds to a distortion of a basic structure. The distortion is defined by a displacement field $\mathbf{u}(\mu, \mathbf{T})$ which can be expressed in the form of a Fourier series. For a one-dimensional INC modulation, the displacement of each atom μ ($\mu = 1, \ldots, s$) in each basic cell T is given by

$$\mathbf{u}(\mu, T) = \mathbf{u}^{\mu}(v = \mathbf{k} \cdot \mathbf{T}), \tag{2}$$

where $\mathbf{u}^{\mu}(v)$ are the atomic modulation functions defined by

$$\mathbf{u}^{\mu}(v) = \tfrac{1}{2} \sum \mathbf{U}_n^{\mu} \exp(2\pi i n v), \tag{3}$$

where $\mathbf{U}_n^{\mu}$ ($n = 0, \pm 1, \pm 2, \ldots$) are complex vectorial amplitudes and v is a continuous variable which corresponds to the so-called internal coordinate in the superspace formalism (Janner & Janssen, 1980). Accordingly, the position of each atom $\mathbf{r}(\mu, \mathbf{T})$ in the INC structure is given by

$$\mathbf{r}(\mu, \mathbf{T}) = \mathbf{r}_b^{\mu} + \mathbf{T} + \mathbf{u}(\mu, \mathbf{T}), \tag{4}$$

where $\mathbf{r}_b^{\mu}$ is the position of atom μ in the basic structure. Similar expressions to (2) and (3) can be considered for the modulated thermal parameters.

With the basic structure known, the structural parameters needed to describe the INC structure are therefore the complex amplitudes involved in (3). In principle, the Fourier series (3) contains infinite terms, but in a practical situation the number of Fourier amplitudes to be considered in the refinement of an INC structure is quite low. It is assumed that the series (3) can be truncated after harmonics of an order equal to the higher order of the measured satellite reflections (van Smaalen *et al.*, 1986; van Aalst, den Hollander, Peterse & de Wolff, 1976).

In general, the mentioned structural parameters are not all independent, but some of them can be related and (or) restricted by superspace symmetry. If we are only concerned with the positional parameters, it can be shown that if $\mathbf{u}^{\mu}(v)$ and $\mathbf{u}^{\nu}(v)$ are the atomic modulation functions of two atoms, μ and ν, symmetry related by $\{R|\mathbf{t}\}$ in the basic structure, then the superspace-group element $\{R|\mathbf{t}, \tau\}$ implies the following relation:

$$\mathbf{u}'^{\nu}(R_I v + \tau_0) = R\mathbf{u}'^{\mu}(v), \tag{5}$$

where $R_I = \pm 1$ if $R\mathbf{k} = \pm\mathbf{k}$, $\tau_0 = \tau + \mathbf{k} \cdot \mathbf{t}$ and

$$\begin{aligned} \mathbf{u}'^{\mu}(v) &= \mathbf{u}^{\mu}(v - \mathbf{k} \cdot \mathbf{r}_b^{\mu}) \\ \mathbf{u}'^{\nu}(v) &= \mathbf{u}^{\nu}(v - \mathbf{k} \cdot \mathbf{r}_b^{\nu}). \end{aligned} \tag{6}$$

Equation (5) expresses the relation between the atomic modulation functions of symmetry-related atoms in the basic structure and in the INC phase, and reduces the number of these functions to an independent set. When relation (5) involves atoms located in special positions in the basic structure ($\mu = \nu$), the atomic modulation functions for these atoms have special forms due to the restrictions appearing on their harmonic amplitudes.

In the basic structure of TMATC-Zn, there are 12 atoms in the asymmetric unit (excluding hydrogens) and, from these, 9 are located in special positions at $x = 0{\cdot}25$ [position 4(*c*) in Wyckoff notation]. Therefore, the successive substitution in (5) of the superspace-group elements (1) reduces to 12 the number of independent atomic modulation functions in the INC structure. From these, those corresponding to the mentioned atoms located in special positions have further restrictions on their harmonic components. Thus, if we consider the element $\{\sigma_x|\frac{1}{2}\,0\,0, \frac{1}{2}\}$ in (5), for one of these atoms it yields

$$\mathbf{u}'^{\mu}(v + \tfrac{1}{2}) = \sigma_x \mathbf{u}'^{\mu}(v), \tag{7}$$

which implies the following restrictions:

x components: $(\mathbf{U}_n^{\mu})_x = 0$ if n = even (8*a*)

y and z components: $(\mathbf{U}_n^{\mu})_{y,z} = 0$ if n = odd. (8*b*)

Similar considerations can be made for the modulated thermal parameters (Yamamoto, 1982*b*; Pérez-Mato, Madariaga, Zuñiga & Garcia-Arribas, 1987).

5. Refinement of the structures

5.1. *The INC structure*

For the refinement of the INC structure, the *REMOS*.82 program (Yamamoto, 1982*a*,*b*) was used. In the Fourier series (3), harmonics are considered up to the same order as the higher order of the measured satellites, that is, second order. In this way, displacements for each atom are due to the zero, first and second harmonics. But for atoms in special positions restrictions (8) reduce the number of amplitudes to be refined. If we separate each amplitude into its real and imaginary parts, we obtain a total of 177 positional amplitudes to be considered in the refinements. For the thermal parameters, only the zero harmonics are considered.

The general minimized function in *REMOS*.82 is $\sum w|\Delta F|^2 / \sum w|F_0|^2$ ($w = 1$ in our refinement). In the structure-factor calculations, the scattering factors used for Zn^{2+}, Cl^-, N and C atoms were those of Cromer & Mann (1968) and anomalous-scattering corrections were performed for Zn and Cl atoms (Cromer & Liberman, 1970).

The integral involved in the structure-factor formula (Yamamoto, 1982*b*) was calculated with a grid of eight points. Starting with the atomic positions of the basic structure, zero values for the modulation amplitudes of all atoms and fixed isotropic temperature factors, the refinement coverged to $R = 0{\cdot}16$. This index reduced to 0·085 on assigning to the atoms

Table 3. *Positional* ($\times 10^4$) *and thermal parameters of the INC structure*

*R*0 are the atomic coordinates in the basic structure. *UI* ($I = 0, 1, 2$) are the modulation amplitudes; Re and Im indicate real and imaginary parts. $U_{eq} = (U_{11} + U_{22} + U_{33})/3$. The e.s.d.'s of the refined parameters are given in parentheses.

		*R*0	*U*0	Re*U*1	Im*U*1	Re*U*2	Im*U*2	U_{eq} (Å^2)
Zn	*x*	2500	0	−101 (7)	−153 (7)	0	0	0·048 (4)
	y	4070	−6 (3)	0	0	5 (3)	−2 (4)	
	z	2454	−14 (5)	0	0	−4 (4)	1 (5)	
Cl(1)	*x*	2500	0	88 (14)	−199 (13)	0	0	0·084 (6)
	y	4063	−12 (5)	0	0	8 (8)	−7 (7)	
	z	650	5 (8)	0	0	8 (9)	−9 (8)	
Cl(2)	*x*	2500	0	−168 (15)	−434 (15)	0	0	0·100 (7)
	y	5420	−4 (6)	0	0	1 (6)	4 (7)	
	z	3136	21 (6)	0	0	10 (9)	2 (9)	
Cl(3)	*x*	442	−7 (10)	−111 (10)	26 (10)	5 (10)	12 (11)	0·093 (5)
	y	3391	10 (4)	−16 (6)	−149 (5)	11 (5)	−1 (5)	
	z	3059	−9 (4)	−41 (6)	29 (6)	−4 (5)	−3 (6)	
N(1)	*x*	2500	0	96 (58)	−148 (58)	0	0	0.160 (9)
	y	950	−119 (23)	0	0	13 (30)	10 (27)	
	z	1484	−97 (25)	0	0	−2 (34)	5 (32)	
C(1)	*x*	2500	0	−78 (46)	31 (46)	0	0	0·070 (3)
	y	977	21 (15)	0	0	1 (21)	6 (23)	
	z	2725	−107 (25)	0	0	8 (32)	9 (33)	
C(2)	*x*	2500	0	−23 (79)	319 (79)	0	0	0.260 (6)
	y	62	−107 (31)	0	0	5 (41)	4 (40)	
	z	1059	62 (35)	0	0	−7 (48)	−15 (46)	
C(5)	*x*	3706	24 (30)	260 (55)	−380 (50)	−27 (39)	−43 (43)	0.170 (5)
	y	1464	−65 (12)	−43 (26)	207 (25)	24 (18)	8 (17)	
	z	967	115 (18)	60 (28)	−102 (28)	−20 (26)	−14 (25)	
N(2)	*x*	2500	0	−138 (50)	−187 (50)	0	0	0.090 (7)
	y	8250	−58 (21)	0	0	31 (29)	41 (27)	
	z	4933	2 (21)	0	0	10 (30)	−51 (31)	
C(3)	*x*	2500	0	496 (52)	132 (51)	0	0	0.080 (5)
	y	8896	−50 (19)	0	0	−7 (26)	47 (27)	
	z	4235	18 (24)	0	0	63 (33)	1 (34)	
C(4)	*x*	2500	0	−136 (46)	25 (45)	0	0	0.090 (5)
	y	7410	−66 (20)	0	0	73 (29)	−56 (27)	
	z	4377	106 (25)	0	0	−54 (35)	74 (35)	
C(6)	*x*	3940	−138 (25)	−325 (42)	−170 (43)	3 (38)	−32 (34)	0.140 (4)
	y	8467	−15 (13)	−149 (20)	−8 (21)	36 (20)	8 (19)	
	z	5374	71 (18)	208 (30)	25 (30)	−1 (25)	−31 (24)	

anisotropic temperature factors* of the basic structure and including them in the refinement. At this point, as some N–C interatomic distances were unreasonable, a distance restriction for these atoms was introduced. The final calculated *R* values for all reflections and unit weights are 0·077, 0·052, 0·121 and 0·49 for all, main, first-order satellite and second-order satellite reflections, respectively. Attempts to refine up to the second-order harmonic excluding second-order satellite reflections produced an increase in the second-harmonic amplitudes and a lower *R* value of 0·06 (0·05 and 0·10 for main and first-order reflections respectively). However, we assume, as stated by van Smaalen *et al.* (1986), that the order up to which satellite reflections are taken into account in the refinement limits the order up to which harmonics can be determined. For this reason, we consider the first refinement (with a higher *R* value) as the final result. Other attempts to refine first-order harmonics with first- and second-order satellites failed. The final structural parameters are given in Table 3 where the basic positions *R*0 correspond to those obtained in our own refinement of the basic structure (phase I).* In Table 3, the Fourier amplitudes correspond to the shifted modulation functions (6) [$\mathbf{U}'^{\mu}_n = \mathbf{U}^{\mu}_n \exp(-2\pi i n \mathbf{k} \cdot \mathbf{r}^{\mu}_b)$].

The high value found for the *R* index of the second-order satellite reflections can be justified by inspecting the *R*-value distribution in terms of $|F_0|$. Such a distribution shows that the *R* value for second-order satellites is similar to the one of main or first-order reflections of similar intensity. Moreover, the list of structure factors shows that, in general, $|\Delta F|$ values for second-order satellites are not greater than those corresponding to first order and main reflections, but their $|F_0|$ values are small and so their relative errors are high.

The variation of the atomic coordinates along the whole crystal can be represented in terms of the atomic modulation functions [see (2)]. From (3) and the atomic parameters of Table 3, the (**a**, *v*) projections (*v* internal coordinate) of the modulation for the *x* atomic coordinates are shown in Fig. 3. In order to show the action of a superspace symmetry operator $\{R|\mathbf{t}, \tau\}$, Fig. 3 shows also the atomic modulation function of Cl(3)′, C(5)′ and C(6)′ atoms which are symmetry related to Cl(3), C(5) and C(6) atoms respectively through the $\{\sigma_x|\frac{1}{2}, 0, 0, \frac{1}{2}\}$ transformation, *i.e.* a reflection through a mirror plane at $x = \frac{1}{4}$ followed by a translation of $\frac{1}{2}$ along the internal coordinate *v*.

An analysis of the atomic parameters of Table 3 shows the most relevant characteristics of the INC modulation of TMATC-Zn, which are also seen in projections like those of Fig. 3. The modulations of the *x* atomic coordinate have the second harmonics restricted by symmetry to zero, except the Cl(3), C(5) and C(6) atoms, for which the second harmonics are negligible against first harmonics. So, it can be said that the *x* component of the modulation of the whole structure is nearly a sinusoidal distortion. Such a characteristic appears clearly in Fig. 3.

For atoms lying on the mirror plane in the basic structure, the *y* and *z* components of their modulations have first-harmonic symmetry restricted to zero and the second harmonics are, in general, small; their atomic modulation functions are then much smaller than those of the *x* coordinate. The *y* and *z* components of the atomic modulations for atoms outside the mirror plane in the basic structure have no restrictions but first harmonics are again larger than second ones. The conclusion is that the most important component of the analysed distortion represents a plane-wave distortion of the *x* atomic parameters of the

* The anisotropic temperature factor employed has the form $\exp(-T)$ where $T = 2\pi^2 \sum_i \sum_j h_i U_{ij} h_j a_i^* a_j^*$ $(i, j = 1, 2, 3)$.

* Lists of structure factors and thermal parameters of the structures reported in this paper have been deposited with the British Library Document Supply Centre as Supplementary Publication No. SUP 43725 (15 pp.). Copies may be obtained through The Executive Secretary, International Union of Crystallography, 5 Abbey Square, Chester CH1 2HU, England.

basic structure. The phase shift between distortions of different atoms can be directly observed from representations like those of Fig. 3 for the x component of the modulation. The x modulations of the Zn, Cl(1) and Cl(2) atoms have nearly the same phase and they are $\pi/2$ shifted with respect to the modulation of the Cl(3) atom. For atoms belonging to the $N(CH_3)_4$ groups, the phase shifts between their modulations are in general not so simple.

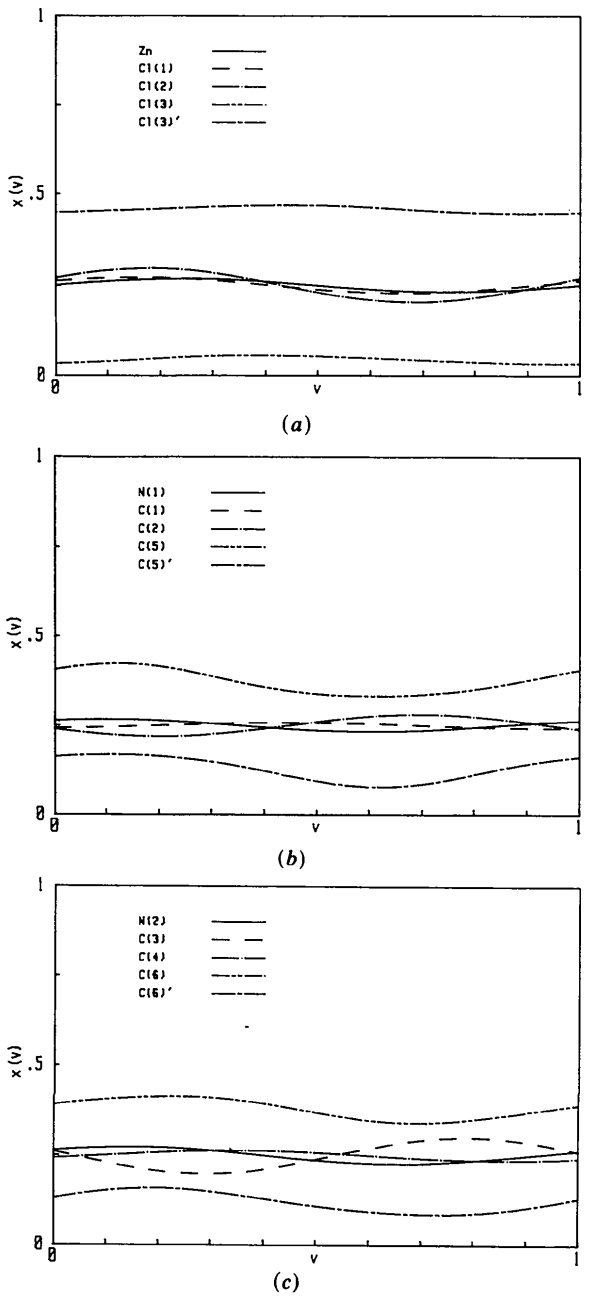

Fig. 3. Modulated atomic position along the internal coordinate v for (a) Zn and Cl atoms, (b) N(1), C(1), C(2) and C(5) atoms, and (c) N(2), C(3), C(4) and C(6) atoms. In each group, symmetry-related atoms by the $\{\sigma_x|\frac{1}{2}, 0, 0, \frac{1}{2}\}$ superspace element are included, to show the meaning of the operation.

The structural distortion and the relative motions of the molecular groups can be visualized in terms of modulated rotations and modulated translations of the $ZnCl_4$ and $N(CH_3)_4$ rigid groups. For these groups, rotations R_x, R_y and R_z around the x, y and z axes, as a function of the internal coordinate v, were calculated by a least-squares fit. The results are shown in Fig. 4. The double-harmonic character shown by the R_x rotation and the simple-harmonic characters of the R_y and R_z rotations (see Fig. 4) should be attributed to the structure superspace symmetry, since (7) can also be considered for a

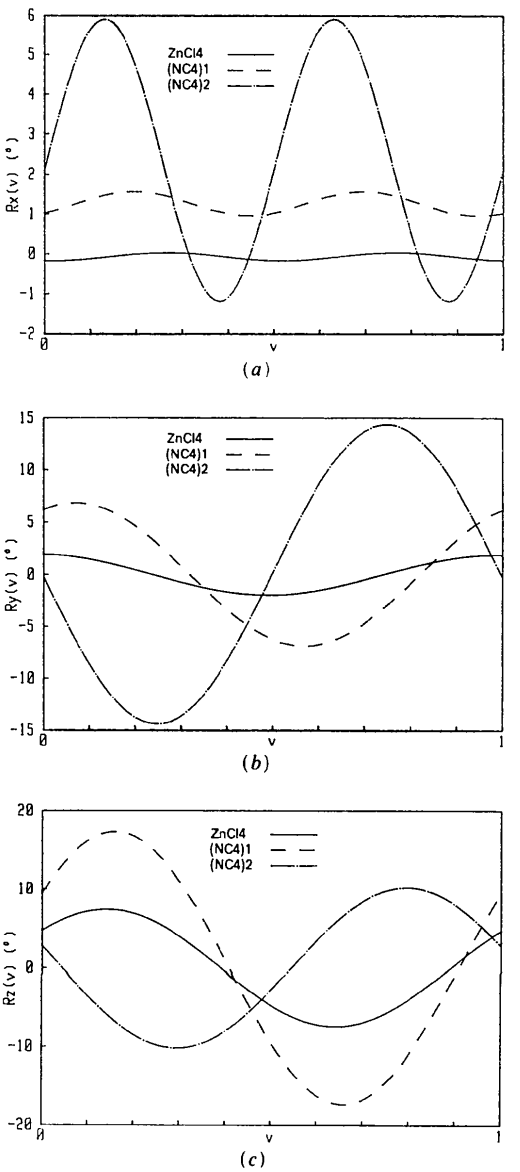

Fig. 4. Modulated rotational angles R_x (a), R_y (b) and R_z (c), around the x, y and z axes, respectively, *versus* the internal coordinate v, calculated with the approximation of rigid $ZnCl_4$ and $[N(CH_3)_4]$ groups. The last ones are referred to in the figures as (NC4)1 and (NC4)2.

Table 4. *Interatomic distances in the INC phase*

D_{av}, D_{max} and D_{min} are the average, maximum and minimum distances, respectively. D_{bas} is the calculated distance in the basic structure and Δ the difference between D_{max} and D_{min}. The distances are given in Å and the e.s.d.'s in parentheses.

	D_{av}	D_{max}	D_{min}	Δ	D_{bas}
Zn–Cl(1)	2·19 (1)	2·20 (2)	2·17 (2)	0·03 (3)	2·216 (7)
–Cl(2)	2·28 (1)	2·30 (2)	2·27 (2)	0·03 (2)	2·261 (7)
–Cl(3)	2·26 (1)	2·28 (2)	2·22 (2)	0·06 (2)	2·258 (6)
N(1)–C(1)	1·54 (6)	1·54 (8)	1·54 (8)	0·0 (1)	1·53 (3)
–C(2)	1·43 (7)	1·4 (1)	1·4 (1)	0·0 (1)	1·48 (4)
–C(5)	1·49 (5)	1·57 (9)	1·37 (9)	0·2 (1)	1·49 (4)
N(2)–C(3)	1·39 (7)	1·41 (9)	1·36 (9)	0·1 (1)	1·32 (6)
–C(4)	1·44 (6)	1·55 (9)	1·35 (9)	0·2 (1)	1·47 (4)
–C(6)	1·41 (4)	1·52 (8)	1·35 (8)	0·2 (1)	1·44 (3)

pseudovector and the restrictions (8) are then interchanged. Note that the associated translation motion T of the rigid groups must show a complementary character, that is, T_x must be a simple-harmonic function, whereas T_y and T_z must be double-harmonic functions.

The decomposition of the structural distortion in terms of rotations and translations is a good approximation for the $ZnCl_4$ groups, but it is not for the organic ones, which do not behave as rigid groups, its structural distortions containing an important molecular deformation component. However, the calculated molecular modulated rotations show clearly the phase and antiphase relations of the different molecular units. For the $ZnCl_4$ group, the most important rotation is R_z, with a maximum amplitude of 7° against 2 and 0·1° for the corresponding R_y and R_x rotations. R_z rotations are in phase for the $ZnCl_4$ and (NC4)1 molecules, but nearly in antiphase with that of the (NC4)2 group. Rotations around the y axis show less-definite phase relations, whereas the R_x rotations have nearly the same phase for all groups.

The interatomic distances are also modulated as they change from cell to cell according to the atomic modulation. The maximum and minimum values of the interatomic distances of bonded atoms in the basic structure and their average values are given in Table 4. The Zn–Cl interatomic distances are in good agreement with those of the basic structure. The N–C distances have high fluctuations (up to 0·2 Å), but they also have associated high standard deviations.

5.2. *The lock-in structure*

The calculation and refinement of the lock-in structure were performed with the *SHELX* program (Sheldrick, 1976). Scattering factors for Zn^{2+}, Cl^-, N and C atoms, as given in Cromer & Mann (1968), and anomalous-dispersion corrections for Zn and Cl atoms (Cromer & Liberman, 1970) were used for the structure-factor calculation. The structure was solved by a least-squares method with a block-diagonal matrix and using as starting parameters those of the basic structure extended to five cells. The refinement

Table 5. *Atomic parameters of the lock-in structure*

To compare coordinates with those of the basic or INC structures, note that the first appended numeral labels the basic subcell. $U_{eq} = (U_{11}+U_{22}+U_{33})/3$. The e.s.d.'s are given in parentheses.

	x	y	z	U_{eq}(Å^2)
Zn(1)	0·25	0·4062 (7)	0·0490 (1)	0·064 (6)
Cl(11)	0·261 (2)	0·406 (1)	0·0129 (2)	0·11 (1)
Cl(12)	0·281 (2)	0·540 (1)	0·0626 (3)	0·11 (1)
Cl(13)	0·036 (2)	0·351 (1)	0·0611 (3)	0·10 (1)
Cl(14)	0·447 (2)	0·323 (1)	0·0615 (3)	0·10 (1)
N(11)	0·259 (6)	0·103 (5)	0·0295 (8)	0·09 (2)
C(111)	0·263 (7)	0·102 (5)	0·0540 (9)	0·06 (3)
C(112)	0·230 (9)	0·013 (5)	0·023 (1)	0·12 (3)
C(113)	0·417 (7)	0·102 (5)	0·023 (1)	0·08 (3)
C(114)	0·205 (9)	0·187 (5)	0·020 (1)	0·14 (3)
N(12)	0·233 (5)	0·831 (3)	0·0988 (7)	0·05 (2)
C(121)	0·163 (6)	0·890 (4)	0·0831 (8)	0·05 (2)
C(122)	0·264 (7)	0·749 (4)	0·087 (1)	0·08 (3)
C(123)	0·387 (6)	0·864 (4)	0·1001 (8)	0·06 (2)
C(124)	0·158 (6)	0·822 (4)	0·1201 (8)	0·06 (2)
Zn(2)	0·2174 (9)	0·4064 (6)	0·2491 (1)	0·042 (5)
Cl(21)	0·217 (2)	0·403 (1)	0·2121 (2)	0·08 (1)
Cl(22)	0·193 (2)	0·541 (1)	0·2629 (3)	0·08 (1)
Cl(23)	0·032 (2)	0·324 (1)	0·2610 (3)	0·08 (1)
Cl(24)	0·439 (2)	0·349 (1)	0·2605 (3)	0·10 (1)
N(21)	0·235 (6)	0·086 (4)	0·2301 (7)	0·01 (2)
C(211)	0·264 (7)	0·101 (5)	0·2535 (8)	0·10 (3)
C(212)	0·285 (7)	−0·001 (4)	0·224 (1)	0·08 (3)
C(213)	0·353 (8)	0·144 (5)	0·222 (1)	0·10 (3)
C(214)	0·085 (8)	0·122 (6)	0·226 (1)	0·18 (4)
N(22)	0·220 (7)	0·830 (5)	0·2978 (9)	0·06 (2)
C(221)	0·198 (9)	0·897 (5)	0·281 (1)	0·13 (3)
C(222)	0·230 (9)	0·744 (5)	0·288 (1)	0·09 (4)
C(223)	0·370 (8)	0·861 (6)	0·302 (1)	0·15 (4)
C(224)	0·099 (7)	0·843 (5)	0·313 (1)	0·09 (3)
Zn(3)	0·240 (1)	0·4059 (6)	0·4493 (1)	0·064 (6)
Cl(31)	0·256 (2)	0·405 (1)	0·4130 (3)	0·12 (1)
Cl(32)	0·268 (2)	0·541 (1)	0·4631 (3)	0·11 (1)
Cl(33)	0·020 (2)	0·352 (1)	0·4600 (3)	0·09 (1)
Cl(34)	0·433 (2)	0·323 (1)	0·4623 (3)	0·11 (1)
N(31)	0·257 (9)	0·094 (6)	0·427 (1)	0·18 (3)
C(311)	0·26 (1)	0·086 (6)	0·451 (1)	0·22 (4)
C(312)	0·229 (8)	0·002 (6)	0·421 (1)	0·14 (3)
C(313)	0·418 (9)	0·108 (5)	0·424 (1)	0·13 (3)
C(314)	0·17 (1)	0·171 (5)	0·418 (1)	0·16 (4)
N(32)	0·250 (6)	0·832 (5)	0·4994 (9)	0·09 (2)
C(321)	0·191 (7)	0·894 (4)	0·483 (1)	0·09 (2)
C(322)	0·253 (9)	0·739 (5)	0·496 (1)	0·15 (4)
C(323)	0·406 (6)	0·857 (3)	0·5016 (7)	0·03 (2)
C(324)	0·146 (7)	0·831 (4)	0·5178 (9)	0·07 (2)
Zn(4)	0·235 (1)	0·4072 (7)	0·6492 (1)	0·063 (6)
Cl(41)	0·229 (2)	0·406 (1)	0·6128 (3)	0·10 (1)
Cl(42)	0·224 (3)	0·545 (2)	0·6632 (4)	0·14 (1)
Cl(43)	0·046 (3)	0·336 (1)	0·6623 (3)	0·12 (1)
Cl(44)	0·454 (2)	0·346 (1)	0·6597 (3)	0·10 (1)
N(41)	0·236 (7)	0·094 (5)	0·6298 (9)	0·09 (2)
C(411)	0·278 (7)	0·103 (5)	0·6529 (9)	0·10 (3)
C(412)	0·244 (8)	0·003 (5)	0·623 (1)	0·11 (3)
C(413)	0·34 (1)	0·158 (6)	0·621 (2)	0·21 (5)
C(414)	0·100 (8)	0·139 (5)	0·622 (1)	0·12 (3)
N(42)	0·240 (7)	0·827 (5)	0·700 (1)	0·12 (2)
C(421)	0·158 (8)	0·884 (4)	0·685 (1)	0·10 (3)
C(422)	0·255 (8)	0·739 (5)	0·692 (1)	0·14 (3)
C(423)	0·392 (7)	0·860 (4)	0·7021 (8)	0·07 (2)
C(424)	0·146 (8)	0·828 (5)	0·720 (1)	0·11 (3)
Zn(5)	0·2191 (9)	0·4063 (7)	0·8493 (1)	0·050 (6)
Cl(51)	0·235 (2)	0·405 (1)	0·8127 (2)	0·10 (1)
Cl(52)	0·210 (3)	0·542 (1)	0·8627 (3)	0·11 (1)
Cl(53)	0·020 (2)	0·335 (2)	0·8602 (3)	0·12 (1)
Cl(54)	0·431 (2)	0·342 (1)	0·8625 (3)	0·11 (1)
N(51)	0·253 (7)	0·101 (5)	0·8298 (8)	0·10 (2)
C(511)	0·273 (6)	0·103 (4)	0·8539 (8)	0·04 (2)
C(512)	0·264 (9)	0·011 (5)	0·822 (1)	0·15 (4)
C(513)	0·355 (8)	0·169 (5)	0·822 (1)	0·10 (3)
C(514)	0·133 (8)	0·155 (5)	0·821 (1)	0·14 (3)
N(52)	0·237 (6)	0·840 (5)	0·8981 (9)	0·09 (2)
C(521)	0·250 (9)	0·889 (5)	0·878 (1)	0·15 (4)
C(522)	0·237 (9)	0·747 (5)	0·894 (1)	0·19 (4)
C(523)	0·386 (7)	0·842 (5)	0·908 (1)	0·09 (3)
C(524)	0·115 (7)	0·858 (5)	0·913 (1)	0·11 (3)

Table 6. *Interatomic distances in the lock-in structure*

The distances are given in Å and the e.s.d.'s in parentheses.

Zn(1)–Cl(11) 2.21 (1)	N(11)–C(111) 1·50 (7)	N(12)–C(121) 1·47 (7)
–Cl(12) 2·24 (2)	–C(112) 1·5 (1)	–C(122) 1·47 (8)
–Cl(13) 2·23 (2)	–C(113) 1·48 (8)	–C(123) 1·47 (7)
–Cl(14) 2·32 (2)	–C(114) 1·5 (1)	–C(124) 1·47 (7)
Zn(2)–Cl(21) 2·27 (1)	N(21)–C(211) 1·48 (7)	N(22)–C(221) 1·5 (1)
–Cl(22) 2·25 (2)	–C(212) 1·47 (9)	–C(222) 1·5 (1)
–Cl(23) 2·22 (2)	–C(213) 1·49 (9)	–C(223) 1·5 (1)
–Cl(24) 2·28 (2)	–C(214) 1·48 (9)	–C(224) 1·46 (9)
Zn(3)–Cl(31) 2·23 (2)	N(31)–C(311) 1·5 (1)	N(32)–C(321) 1·47 (9)
–Cl(32) 2·27 (2)	–C(312) 1·5 (1)	–C(322) 1·5 (1)
–Cl(33) 2·24 (2)	–C(313) 1·5 (1)	–C(323) 1·46 (8)
–Cl(34) 2·30 (2)	–C(314) 1·5 (1)	–C(324) 1·47 (8)
Zn(4)–Cl(41) 2·23 (2)	N(41)–C(411) 1·47 (8)	N(42)–C(421) 1·47 (9)
–Cl(42) 2·30 (3)	–C(412) 1·5 (1)	–C(422) 1·5 (1)
–Cl(43) 2·18 (2)	–C(413) 1·5 (1)	–C(423) 1·47 (9)
–Cl(44) 2·28 (2)	–C(414) 1·5 (1)	–C(424) 1·47 (9)
Zn(5)–Cl(51) 2·25 (1)	N(51)–C(511) 1·49 (7)	N(52)–C(521) 1·5 (1)
–Cl(52) 2·26 (2)	–C(512) 1·5 (1)	–C(522) 1·5 (1)
–Cl(53) 2·20 (2)	–C(513) 1·5 (1)	–C(523) 1·47 (8)
–Cl(54) 2·29 (2)	–C(514) 1·48 (9)	–C(524) 1·46 (8)

was accomplished with unit weights, anisotropic thermal parameters for Zn and Cl atoms, and isotropic ones for N and C atoms. The final residual based on F values was $R = 0{\cdot}075$. The final atomic parameters of the lock-in phase of TMATC-Zn are given in Table 5, and the interatomic distances in Table 6.

6. Comparison of the structures

The structures of the INC and lock-in phases reported above have been determined by two independent methods. The INC distortion has been refined using the superspace description with a modulation including three harmonics (zero, first and second order), and restricted by the superspace group $P(Pmcn):(s, 1, -1)$. On the other hand, the structure of the lock-in phase has been determined by standard crystallographic methods, taking the basic structure (phase I) as the starting point of the refinement process, and the space group $P2_1cn$ for the required structure.

Given the INC character, the two structures cannot be directly compared. However, a comparable commensurate structure can be constructed from the determined INC structure by changing only the modulation wave vector to its lock-in value of $\frac{2}{5}\mathbf{c}^*$. From (2), the structural distortion is then repeated every five basic cells along the z axis. Thus, only the values of the atomic modulation functions at five equidistant points (distance $\frac{1}{5}$) along v, corresponding to the five cells, are relevant for describing the structure. If we further impose that the resulting commensurate structure has the space group of the lock-in phase, the value v_0, which can be assigned to the first of the five cells, is restricted to the values $\frac{1}{4}+(n/10)$ (n = integer). This result can be obtained, for instance, using the superspace symmetry relations between the atomic modulation functions and checking the resultant space-group symmetry operations for the five discrete values which determine the commensurate structure. The value for v_0 is in agreement with the fact indicated in Table 2 that the phase of the order parameter, which for this purpose can be identified with the internal coordinate (Pérez-Mato *et al.*, 1984*a*), should have the value $\pi/2$ in the lock-in phase. The different possibilities given by the choice of n in the expression for v_0 correspond to the different equivalent domain choices for relating the basic and the lock-in structure.

With these considerations and the periodicity of the modulation functions taken into account, the INC and lock-in distortions of the Zn and Cl positions are compared in Fig. 5. The atomic displacements in the five basic subcells of the lock-in structure are put at

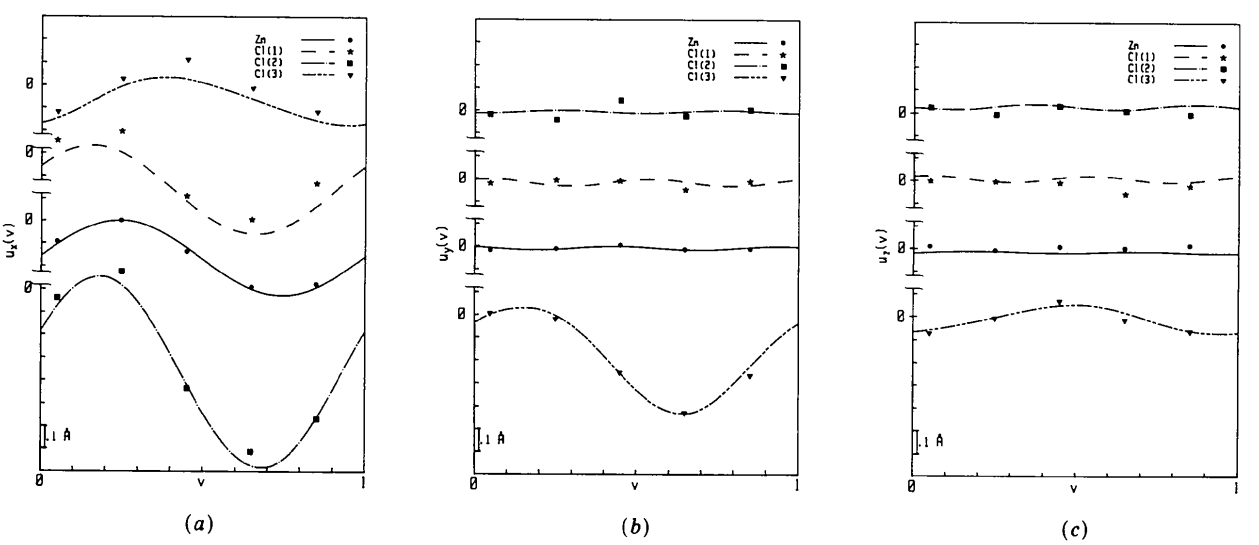

Fig. 5. Atomic displacement modulation function along the x (*a*), y (*b*) and z (*c*) axes of the Zn and Cl atoms, in the INC structure (curves) compared with the corresponding displacement of the lock-in structure (discrete points).

Table 7. *Amplitudes* ($\times 10^4$) *of the modes describing the lock-in distortion*

	$A_{1g}(x)$	$A_{1g}(y)$	$A_{1g}(z)$	$B_{2u}(x)$	$B_{2u}(y)$	$B_{2u}(z)$	$\Sigma_1^1(x)$	$\Sigma_1^2(x)$	$\Sigma_1^1(y)$	$\Sigma_1^2(y)$
Zn		−6	5	−178					−1·5	−2·1
Cl(1)		−11·6	−15	−103·4					4·7	0·7
Cl(2)		−3·8	9	−148					−5·4	−2·3
Cl(3)	7·8	−8·9	−3·5	−142·2	14·1	−9·5	−6·8	−3·1	−2·7	−2·9
N(1)		6·8	−20	−21·8					24·8	8·2
N(2)		70	11	−142·8					16·1	19·9
C(1)		12	−90	167·8					−25·6	−16·8
C(2)		−2·6	64	4·6					15·1	8·2
C(3)		−0·6	−12·5	−578					3·4	15
C(4)		25·8	193	−19·6					2·8	1·2
C(5)	−19·2	−4·6	128·5	81·6	−93·7	21·5	−38·1	−16·4	−6·6	18·7
C(6)	152·9	5·9	121	105	100·7	−351	1	55·3	−7·5	23·7

	$\Sigma_1^1(z)$	$\Sigma_1^2(z)$	$\Sigma_2^1(x)$	$\Sigma_2^2(x)$	$\Sigma_2^1(y)$	$\Sigma_2^2(y)$	$\Sigma_2^1(z)$	$\Sigma_2^2(z)$	$\Sigma_3^1(x)$	$\Sigma_3^2(x)$
Zn	0	−2·5	−3i	−1·2i					−41·1i	−77·5i
Cl(1)	9	4	0·8i	−16·6i					57·8i	−99i
Cl(2)	−1·5	−1·5	−25i	−5·4i					−78·9i	−225i
Cl(3)	5·5	1·5	9·9i	−1i	−7·7i	−0·4i	3·5i	5i	−62·5i	15·5i
N(1)	−24·5	−23	6·5i	−22·7i					44·3i	−52i
N(2)	2·5	−19·5	42·8i	23·9i					−14·7i	−47·1i
C(1)	−18·5	−9	43·9i	−7·9i					−16·6i	29·8i
C(2)	−11	−25	−26·5i	−29·6i					−14·5i	145·8i
C(3)	−3	−72·5	32·5i	−62·9i					220·1i	−19·8i
C(4)	60·5	50·5	16i	−3·3i					−74·3i	−43·3i
C(5)	−17·5	−15·5	−48·9i	−65·2i	43·7i	34i	5i	10·5i	118·1i	−228i
C(6)	8·5	−13·5	41·4i	15·7i	−19·2i	21·3i	11·5i	−23i	−87·1i	−52·7i

	$\Sigma_3^1(y)$	$\Sigma_3^2(y)$	$\Sigma_3^1(z)$	$\Sigma_3^2(z)$	$\Sigma_4^1(x)$	$\Sigma_4^2(x)$	$\Sigma_4^1(y)$	$\Sigma_4^2(y)$	$\Sigma_4^1(z)$	$\Sigma_4^2(z)$
Zn							−0·5	1·6	−2·5	2
Cl(1)							0·2	5·4	−2·5	5
Cl(2)							−4·8	10·5	−7·5	1·5
Cl(3)	−7i	−76·7i	−26·5i	18i	1·3	−1·4	−4·1	9·4	4	3·5
N(1)							22·4	24·9	24·5	10·5
N(2)							14·4	6·2	−12·5	16·5
C(1)							32	14·7	37·5	4·5
C(2)							26·7	19·7	11·5	4·5
C(3)							−6·5	−27·3	−44·5	−3
C(4)							26·8	−10·6	−49·5	79·5
C(5)	−48·6i	142·6i	39i	−46i	−36·8	−40·3	13·1	64·2	1·5	−20
C(6)	−62i	13·5i	88·5i	−3·5i	−15·7	1·7	2·4	−8·2	14	31

the values 0·05, 0·25, 0·45, 0·65 and 0·85 in such a way that they correspond to the subcells 2, 0, 3, 1 and 4, respectively. They can be compared in Fig. 5 with the corresponding atomic modulation functions of the INC structure, defined for all values of v.*

From Fig. 5, the essential coincidence between both distortions for the most significant modulations (those with higher amplitudes) is obvious. This fact can be understood by considering the characteristic features of a lock-in phase, where the primary distorting mode is identified by continuity with the soft-mode of the preceding INC phase. Hence, it is expected that this main distorting mode essentially maintains its 'structure' through the lock-in phase transition except for the change of the modulation vector.

7. Symmetry mode analysis

A more quantitative comparison of the structures can be performed by means of a symmetry mode analysis similar to the one reported for K_2SeO_4 by Pérez-Mato, Gaztelua, Madariaga & Tello (1986). In such an analysis, the distortion relating the lock-in and basic structures is decomposed in terms of symmetry modes of the latter. By this means, the relative weight of the different mode symmetries in the total distortion is revealed. On the other hand, the superspace symmetry for the INC phase implies that each harmonic of the modulation functions describing the INC distortion corresponds to a certain symmetry mode. Therefore the amplitudes of the symmetry modes in the lock-in distortion can be compared with the atomic modulation amplitudes of the INC phase. In the following, we briefly report the results of such an analysis.

From the basic structure, its symmetry and the space group of the lock-in phase, the lock-in distortion can be expressed for each set of symmetry-related atoms in special positions in terms of the following symmetry modes:

$$A_{1g}(y)+A_{1g}(z)+B_{2u}(x)+2\Sigma_1(y)+2\Sigma_1(z)+2\Sigma_2(x)+2\Sigma_3(x)+2\Sigma_4(y)+2\Sigma_4(z),$$

where Σ_1, Σ_3 (Σ_2, Σ_4) correspond to a wave vector $\frac{2}{5}\mathbf{c}^*$ ($\frac{1}{5}\mathbf{c}^*$), and the displacement direction for each mode is indicated in parentheses. Similarly, the displacements in the lock-in phase for each group of eight symmetry-related atoms in general positions can be decomposed into thirty symmetry-mode

* The modulation functions for the x components have been translated along the x axis so that the INC Zn displacement at $v = 0{\cdot}25$ coincides with that of the lock-in phase. This is allowed by the arbitrary position along the x axis of the cell origin in the lock-in phase.

Table 8. *Amplitudes* ($\times 10^4$) *and phases* (°) *of the modes* A_{1g}, $\sum_3$ *and* $\sum_4$ *in the lock-in and INC structures*

For each atom the first and second rows correspond to the values in the INC and lock-in structures, respectively.

	$A_{1g}(x)$	$A_{1g}(y)$	$A_{1g}(z)$	$\sum_3(x)$	$\sum_3(y)$	$\sum_3(z)$	$\sum_4(x)$	$\sum_4(y)$	$\sum_4(z)$
Zn		−6	−14	92|237°				3|22°	2|166°
		−6	5	88|242°				2|107°	5|141°
Cl(1)		−12	5	109|294°				5|319°	6|312°
		−12	−15	115|300°				5|88°	5|117°
Cl(2)		−4	21	233|249°				2|76°	5|11°
		−4	9	238|251°				12|115°	10|169°
Cl(3)	−7	10	−9	57|167°	75|264°	25|145°	7|67°	6|355°	3|217°
	8	−9	−4	64|166°	77|265°	32|124°	2|313°	10|114°	5|41°
N(1)		−119	−97	89|303°				8|38°	3|112°
		7	−20	68|310°				33|48°	27|23°
N(2)		−58	2	116|234°				26|53°	26|281°
		70	11	49|253°				16|23°	21|127°
C(1)		21	−107	42|158°				3|81°	6|48°
		12	−80	34|119°				35|25°	38|7°
C(2)		−107	62	160|94°				3|39°	8|245°
		−3	64	147|96°				33|36°	12|21°
C(3)		−50	18	257|15°				24|98°	32|1°
		−1	−13	221|355°				28|257°	45|184°
C(4)		−66	106	69|170°				46|323°	46|126°
		26	193	86|210°				29|338°	94|122°
C(5)	24	−65	115	230|304°	106|102°	59|300°	25|302°	13|18°	12|215°
	−19	−5	129	257|297°	151|109°	60|310°	55|228°	66|78°	20|274°
C(6)	−138	−15	71	183|208°	75|183°	105|7°	16|275°	18|13°	16|268°
	−153	6	121	102|211°	63|168°	89|358°	16|174°	9|286°	34|66°

contributions:

$$\begin{aligned} &A_{1g}(x)+A_{1g}(y)+A_{1g}(z)+B_{2u}(x)+B_{2u}(y)\\ &\quad+B_{2u}(z)+2\sum_1(x)+2\sum_1(y)+2\sum_1(z)\\ &\quad+2\sum_2(x)+2\sum_2(y)+2\sum_2(z)\\ &\quad+2\sum_3(x)+2\sum_3(y)+2\sum_3(z)\\ &\quad+2\sum_4(x)+2\sum_4(y)+2\sum_4(z), \end{aligned}$$

where again the wave vector of the modes $\sum_1, \sum_3$ ($\sum_2, \sum_4$) is $\frac{2}{5}\mathbf{c}^*$ ($\frac{1}{5}\mathbf{c}^*$). Taking into account that there are nine atoms in special positions and three in a general one in the asymmetric unit of the basic structure, the number of symmetry-mode amplitudes describing the distortion is then 225, in agreement with the number of free structural atomic coordinates in the lock-in phase.

The arbitrariness in the choice of symmetry modes when there exist two for the same displacement direction has been solved by choosing one real and the other imaginary. Their norm has been chosen such that the amplitude of the atomic displacements is unity in the metric of the Bravais lattice corresponding to the lock-in phase, except for the z direction where one fifth of the cell parameter is taken as length unit.

By means of a procedure analogous to the one explianed by Pérez-Mato *et al.* (1986), the amplitude of each symmetry mode participating in the lock-in distortion can be determined using their orthogonality properties. The results are shown in Table 7. It can be seen that a distortion of symmetry $\sum_3$ ($\frac{2}{5}\mathbf{c}^*$) clearly predominates in agreement with the fact that $\sum_3$ is the symmetry of the order parameter in the INC phase. However, modes of symmetry B_{2u} corresponding to the spontaneous polarization and $\sum_2$ also have considerable amplitudes.

On the other hand, in the INC structure, the superspace group $P(Pmcn)$: $(s, 1, -1)$ implies that the successive harmonics n in the atomic modulation functions correspond to symmetry modes transforming according to the following irreducible representations:

$n=0$	A_{1g}
$n=10m\ (m\neq 0)$	$\sum_1$–$A_{1g}(0)$
$n=10m\pm 1$	$\sum_3$–$\sum_3$ ($\frac{2}{5}\mathbf{c}^*$)
$n=10m\pm 2$	$\sum_4$–$\sum_4$ ($\frac{1}{5}\mathbf{c}^*$)
$n=10m\pm 3$	$\sum_2$–$\sum_2$ ($\frac{1}{5}\mathbf{c}^*$)
$n=10m\pm 4$	$\sum_1$–$\sum_1$ ($\frac{2}{5}\mathbf{c}^*$)
$n=10m\pm 5$	$\sum_3$–$B_{2u}(0)$,

where we have also indicated the compatibility relations with the symmetry modes in the lock-in phase. As only harmonics up to second order have been refined in the INC phase, the symmetry of the corresponding distortion can be expressed as $A_{1g}+\sum_3+\sum_4$. From the reference cited above, the amplitudes for the first ($\sum_3$) and second ($\sum_4$) harmonics can be expressed in terms of a modulus and a complex phase. The same can be done with the amplitudes for the modes $\sum_3$ and $\sum_4$ in Table 7. The results, including the value for the A_{1g} modes (which do not need any transformation) are shown for comparison in Table 8. They indicate in general a high correlation between the distortion mode in both structures. In particular, the primary mode $\sum_3$, predominant in the distortion,

maintains essentially the same structure in both phases, as is graphically shown in Fig. 6, where the moduli and phases of the $\sum_3$ modes in the lock-in phase are represented against the corresponding ones in the INC phase. An important point is that the slope of the fitted line in Fig. 6 is 1·02, indicating that the $\sum_3$ distortion also maintains its global amplitude practically constant through the phase transition.

Modes of symmetry A_{1g} and $\sum_4$ in both phases do not exhibit such a clear relation. However, their amplitudes are not so significant when compared with the standard deviations in the structure determination.

Summarizing, we have shown that both the determined INC and lock-in structures of TMATC-Zn are mainly constituted by a distortion of symmetry $\sum_3$, corresponding to the symmetry of the order parameter of the INC phase. This distortion is essentially identical in both structures except for the change in the modulation wave vector. The other secondary modes present in both distortions are not so clearly related, but their reliability is limited given their minor amplitudes. One should also note the considerable importance of a secondary distortion B_{2u} in the lock-in phase, directly related with the spontaneous polarization, while the corresponding mode (fifth harmonic) is not present in the INC phase.

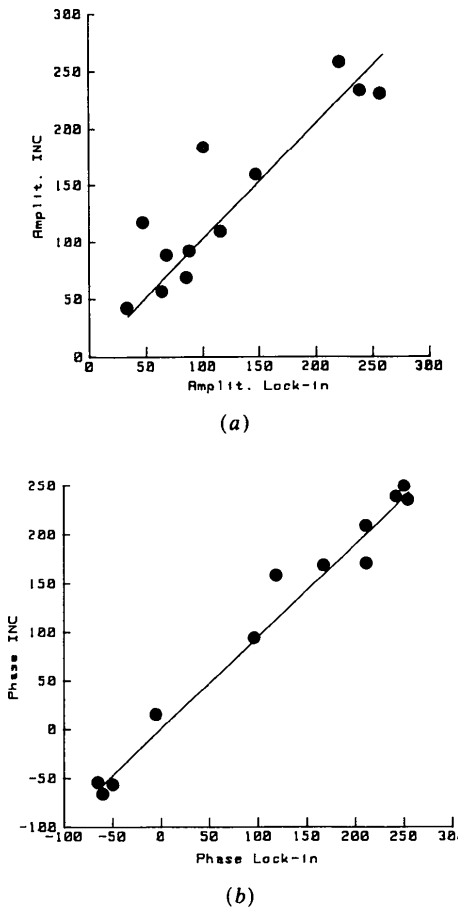

Fig. 6. Representation of the moduli (*a*) and phase (*b*) of the $\sum_3$ modes in the INC structure against the corresponding ones of the lock-in one.

This work was supported by the CAICYT (Spain) project No. 0906-84. We are grateful to A. Yamamoto for supplying his program *REMOS*.82, and gratefully acknowledge the advice of A. Perez Morosov during its implementation. We also extend our gratitude to J. A. Zubillaga for his helpful assistance in the computing work and to G. Chapuis for his hospitality in the Institut de Cristallographie (Université de Lausanne), where the measurements were performed.

References

AALST, W. VAN, DEN HOLLANDER, J., PETERSE, W. J. A. M. & DE WOLFF, P. M. (1976). *Acta Cryst.* B**32**, 47-58.

ALMAIRAC, R., RIBET, M., RIBET, J. L. & BZIOUET, M. (1980). *J. Phys. (Paris)*, **41**, L-315-L-318.

BLINC, R., BURGAR, M., SLAK, J., RUTAR, V. & MILIA, F. (1979). *Phys. Status Solidi A*, **56**, K65-K69.

CROMER, D. T. & LIBERMAN, D. (1970). *J. Chem. Phys.* **53**, 1891-1898.

CROMER, D. T. & MANN, J. B. (1968). *Acta Cryst.* A**24**, 321-324.

DAM, B. & JANNER, A. (1986). *Acta Cryst.* B**42**, 69-77.

GESI, K. & IIZUMI, M. (1980). *J. Phys. Soc. Jpn*, **48**, 337-338.

HENOCQUE, J., SAUVAJOL, J. L., LEFEBVRE, J. & MARION, G. (1983). *J. Raman Spectrosc.* **14**, 93-95.

IIZUMI, M. (1981). JAERI Report M-9843. Japan Atomic Energy Research Institute, Ibaraki, Japan.

JANNER, A. & JANSSEN, T. (1977). *Phys. Rev. B*, **15**, 643-658.

JANNER, A. & JANSSEN, T. (1980). *Acta Cryst.* A**36**, 399-408.

KARAJAMAKI, E., LACHO, R. & LEVOLA, T. (1983). *J. Phys. C*, **16**, 6531-6538.

MACHIDA, M., SUHARA, M., AONO, S. & KOBAYASHI, T. (1983). *Phase Transitions*, **3**, 227-239.

MARION, G. (1981). *J. Phys. (Paris)*, **42**, 469-472.

MASHIYAMA, H. (1980). *J. Phys. Soc. Jpn*, **40**, 2270-2277.

MASHIYAMA, H. & TANISAKI, S. (1980). *Phys. Lett. A*, **76**, 347-349.

PARLINSKI, K. & DENOYER, F. (1985). *J. Phys. C*, **18**, 293-308.

PÉREZ-MATO, J. M., GAZTELUA, F., MADARIAGA, G. & TELLO, M. J. (1986). *J. Phys. C*, **19**, 1923-1935.

PÉREZ-MATO, J. M., MADARIAGA, G. & TELLO, M. J. (1984*a*). *Phys. Rev. B*, **30**, 1534-1553.

PÉREZ-MATO, J. M., MADARIAGA, G. & TELLO, M. J. (1984*b*). *Ferroelectrics*, **53**, 293-296.

PÉREZ-MATO, J. M., MADARIAGA, G., ZUÑIGA, F. J. & GARCIA ARRIBAS, A. (1987). *Acta Cryst.* A**43**, 216-226.

RUIZ-LARREA, I., LOPEZ-ECHARRI, A. & TELLO, M. J. (1981). *J. Phys. C*, **14**, 3171-3176.

SCHWARZENBACH, D. (1977). 4th Eur. Crystallogr. Meet., Oxford. Abstract PI20.

SHELDRICK, G. M. (1976). *SHELX*. Program for crystal structure determination. Univ. of Cambridge, England.

SMAALEN, S. VAN, BRONSEMA, K. D. & MAHY, J. (1986). *Acta Cryst.* B**42**, 43-50.

TANISAKI, S. & MASHIYAMA, H. (1980). *J. Phys. Soc. Jpn*, **48**, 339-340.

WIESNER, J. R., SRIVASTAVA, R. C., KENNARD, C. H. L., DI VAIRA, M. & LINGAFELTER, E. C. (1967). *Acta Cryst.* **23**, 565-574.

WOLFF, P. M. DE (1974). *Acta Cryst.* A30, 777-785.
WOLFF, P. M. DE (1977). *Acta Cryst.* A33, 493-497.
WOLFF, P. M. DE, JANSSEN, T. & JANNER, A. (1981). *Acta Cryst.* A37, 625-636.
YAMAMOTO, A. (1980). *Phys. Rev. B*, **22**, 373-379.
YAMAMOTO, A. (1982*a*). *REMOS*.82. A computer program for refinement of modulated structures. National Institute for Research in Inorganic Materials, Sakura-mura, Niihari-gun, Ibaraki 305, Japan.
YAMAMOTO, A. (1982*b*). *Acta Cryst.* A38, 87-92.

Acta Cryst. (1987). B43, 368-376

LEED Intensity Analysis of the Structure of Coadsorbed Benzene and CO on Rh(111)

BY R. F. LIN,* G. S. BLACKMAN, M. A. VAN HOVE† AND G. A. SOMORJAI

Materials and Molecular Research Division, Lawrence Berkeley Laboratory, and Department of Chemistry, University of California at Berkeley, Berkeley, California 94720, *USA*

(*Received* 27 *October* 1986; *accepted* 24 *March* 1987)

Abstract

The structure of benzene coadsorbed with CO on Rh(111) has been analyzed using low-energy electron diffraction (LEED) interpreted by dynamical calculations. The present structure, Rh(111)-(3×3)-C_6H_6+2CO, complements an earlier result for the system Rh(111)-$\binom{31}{13}$-C_6H_6+CO, but is distinguished by a different ratio of benzene to CO molecules. The main characteristics of the molecule–metal bonding are substantially confirmed: intact benzene lying flat and centered over h.c.p.-type hollow sites with an expanded C_6 ring, and CO standing upright on the same type of hollow site. These two structures are also compared and contrasted with a recent analysis of the structure of benzene coadsorbed with CO on Pt(111), for which bridge sites occur and a larger C_6 ring expansion is found.

1. Introduction

As part of an ongoing study of the structural chemistry of hydrocarbons on transition metal surfaces, we report two structures of benzene adsorbed on the Rh(111) single-crystal surface in the presence of coadsorbed carbon monoxide. The first structure, Rh(111)-$\binom{31}{13}$-C_6H_6+CO, has already been published (Van Hove, Lin & Somorjai, 1983, 1986) and is recalled here for comparison [the $\binom{31}{13}$ matrix notation is equivalent to the $c(2\sqrt{3}\times4)$rect notation, also used in these references]. The second structure, Rh(111)-(3×3)-C_6H_6+2CO, is new and substantially confirms important aspects of the first structure.

Many techniques have been used to study benzene on transition metal surfaces (Nyberg & Richardson, 1979; Tsai & Muetterties, 1982; Massardier, Tardy, Abon & Bertolini, 1983; Surman, Bare, Hofmann & King, 1983; Koel, Crowell, Mate & Somorjai, 1984; Neumann, Mack, Bertel & Netzer, 1985). Our work is based primarily on low-energy electron diffraction (LEED) and high-resolution electron-energy-loss spectroscopy (HREELS). As was observed by thermal desorption spectroscopy (TDS) and HREELS (Mate & Somorjai, 1985), the (3×3) benzene structure on Rh(111) differs from the $\binom{31}{13}$ structure in the molecular ratio C_6H_6:CO, namely 1:2 *vs.* 1:1, respectively.

There also exists a CO-free ordered benzene structure on Rh(111), with a $(2\sqrt{3}\times3)$ rect $=\binom{44}{22}$ superlattice (Mate & Somorjai, 1985). Although this structure has not been analyzed in detail, its principal features are known and provide an interesting comparison with the CO coadsorbate systems. Furthermore, a parallel sequence of benzene/CO structures exists on Pt(111) (Gland & Somorjai, 1973; Mate & Somorjai, 1985), one of which has been structurally analyzed in detail (Ogletree, Van Hove & Somorjai, 1987). The interaction between the coadsorbates can manifest itself both in ordering and in bonding effects: the long-range order depends on the relative coverage of the two coadsorbed molecules, and each molecule bonds very differently to the metal in the absence of the other molecule.

2. LEED analysis of the (3×3) structure

2.1. *LEED experiment*

The Rh(111) single-crystal surface was cleaned by repeated cycles of heating in oxygen, argon sputtering and annealing (Lin, Koestner, Van Hove & Somorjai, 1983). Cleanliness was verified by Auger electron spectroscopy. The data used for this surface structure analysis were obtained at normal incidence. The crystal was oriented to within ~0·2° of normal incidence

* Permanent address: Department of Physics, Fudan University, Shanghai, People's Republic of China.
† Direct inquiries about computational details to this author.

0108-7681/87/040368-09$01.50